Shahid Chamran University of Ahvaz

Journal of Advanced Mathematical Modeling
ISSN (print): 2251-8088, ISSN (on-line): 2645-6141
Vol. 13 No. 5 (2024), pp. 86-98.
DOI: 10.22055/JAMM.2024.45670.2243.

A FLUENCE MAP OPTIMIZATION IN IMRT FOR HEAD AND NECK CANCER BASED ON TRAPEZOIDAL FUZZY NUMBERS

OMOLBANIN BOZORG, ALIREZA FAKHARZADEH JAHROMI* AND ALI DELAVAR KHALAFI

Communicated by: M.H. Farahi

Abstract. The study of clinical observations in the family planning of intensity-modulated radiation therapy (IMRT), indicates that the target dose prescribed within the framework of trapezoidal fuzzy numbers more closely matches the oncologist's goals. In this study, optimal treatment planning was described as a solution to an optimization problem using a quadratic objective function, where the prescribed target dose is a trapezoidal fuzzy number. First, the problem was transformed into a non-fuzzy optimization problem, then the optimal solution was obtained based on the gradient method and projection operations. In this paper, we used Computational Entertainment for Radiotherapy Research (CERR) for treatment planning, importing the patient scans, and calculating the influence matrix. Numerical simulation was performed for a head and neck cancer case. Numerical results were presented in the form of Dose-Volume Histograms (DVH) and compared with the deterministic state. These results showed that the treatment planning that we provided based on the trapezoidal fuzzy target dose, is more consistent with the goals of oncologists.

1. Introduction

Intensity-modulated radiation therapy (IMRT) is a state-of-the-art technique for administering radiation to cancer patients. To achieve a terminal tumor dose, the surrounding

MSC(2020): 00A09, 54C40.

Keywords: IMRT, DVC, trapezoidal fuzzy number, CERR, Sensitivity-Driven Greedy algorithm

Received: 28 December 2023, Accepted: 28 April 2024.

*Corresponding author.

critical organs are inevitably harmed. In this regard, the damaged healthy tissue in this process would be carefully controlled.

Linear accelerator (LINAC) is the primary delivery tool for IMRT that rotates on a gantry around the patient, emitting modulated beams of X-rays from a number of prefixed angles. This modulation is accomplished by means of a device known as a multileaf collimator (MLC). The MLC shapes the pattern of the outgoing radiation beam, in order to precisely target the tumors while minimizing exposure of the neighboring healthy tissues (see Figure 1).

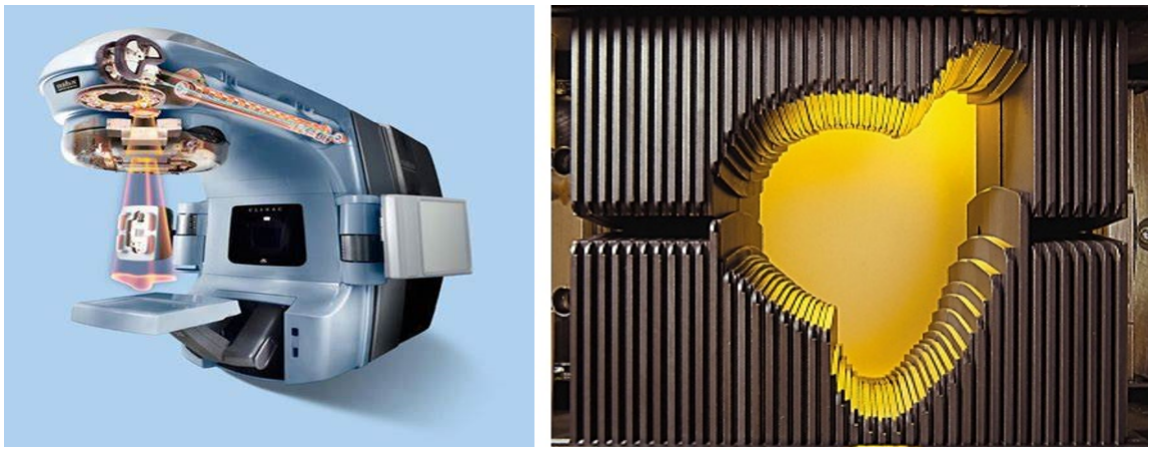

FIGURE 1. left) A LINAC system; right) An MLC system.

It is necessary to determine that how the intensity of an X-ray beam should be at each point (x, y) on the MLC aperture surface for all gantry angles. These fluence maps are represented by nonnegative functions $I_a(x, y)$ for $a = 1, 2, \ldots, k$ where k is the number of gantry angles in use. $I_a(x, y)$ Could be approximated by a set of discrete values $I_a(x_i, y_i)$ with discretizing the MLC aperture by nods (x_i, y_i); thus, one can show the unknown beamlet intensity as $I_a(x_i, y_i), a = 1, 2, \ldots, k$.

2. Dose-Volume Constraints

Radiation oncologists introduce, so-called, dose-volume constraints (DVCs), which specify a given percentage of volume for each critical organ that can be sacrificed, if necessary, while the tumor gives a prescribed amount of radiation. The region of treatment is discretized into small three-dimensional rectangular elements, say voxels. If the absorbed dose values is defined by the voxels with a vector $d \in \mathbb{R}^m_+$ (m is the total number of voxels

in the treatment region), in a standard IMRT model we have $d_i = \sum_{j=1}^{n} a_{ij}x_j$ in which a_{ij} gives the dose absorbed by the i voxel per unit intensity emission from the j-th beamlet. In this regard, matrix $A = (a_{ij}) \in \mathbb{R}_{+}^{(m_t+m_h)}$nis called the influence matrix (m_t and m_h are the number of targets and critical structure voxels, respectively); therefore, $d = Ax$. Since calculating A is quite expensive, currently dose calculation is still considered an important research area. Here, we assume that A is provided by CERR software (Deasy 2006). We remind that for each structure, there is at least one dose-volume constraint. For example, in a sample prescription for lung cancer, the heart DVC specifies that no more than 40 % of the voxels in the heart may exceed a 38 Gray dose.

For fluence optimization, several classes of optimization models have been proposed: linear models (Fakharzadeh, Bozorg, et al. 2011; Cotrutz, Lahanas, et al. 2001), mixed integer programming (Shepard, Ferris, et al. 1999; Sadegheih, Savari, et al. 2018), multi-objective optimization models with Pareto solution (Breedveld, Storchi, et al. 2012; Teichert, Currie, et.al. 2019; Ripsman, Rahimi, et al. 2023) and metaheuristic algorithm (Webb, 1989; Freitas, Oliveira, et al. 2020; Fallahi, Mahnam, et al. 2022). Moreover, recent attempts have been made to use artificial intelligence to solve these problems (see Sevarajan, Manoharan, et al. 2022; Shitharth, Yonbawi, et al. 2023; Devarajan, Alex, et al. 2022; Fu, Zhang, et al. 2021).

But in all such literature, variables, and parameters are considered as a certain kind; even in the real world, many of them are fuzzy, like the prescribed target dose vector parameter. Finding the best influence treatment map in such a situation precisely is our main attention in this paper. The flowchart for IMRT treatment planning on a fuzzy state is given in Figure 2.

3. Problem Formulation

Let $D_v \subset \mathbb{R}_{+}^{m}$ be the set of dose vectors that satisfy all the dose-volume constraints for a given problem and $\tilde{b}_t \in \mathbb{R}_{+}^{m_t}$ be fuzzy prescribed target dose vector; also we assume that the rows of A are organized such that $A^T = [A_t^T A_h^T]$, where A_t is the submatrix consisting of target voxel rows and likewise A_h is made up of healthy tissue voxel rows; then the

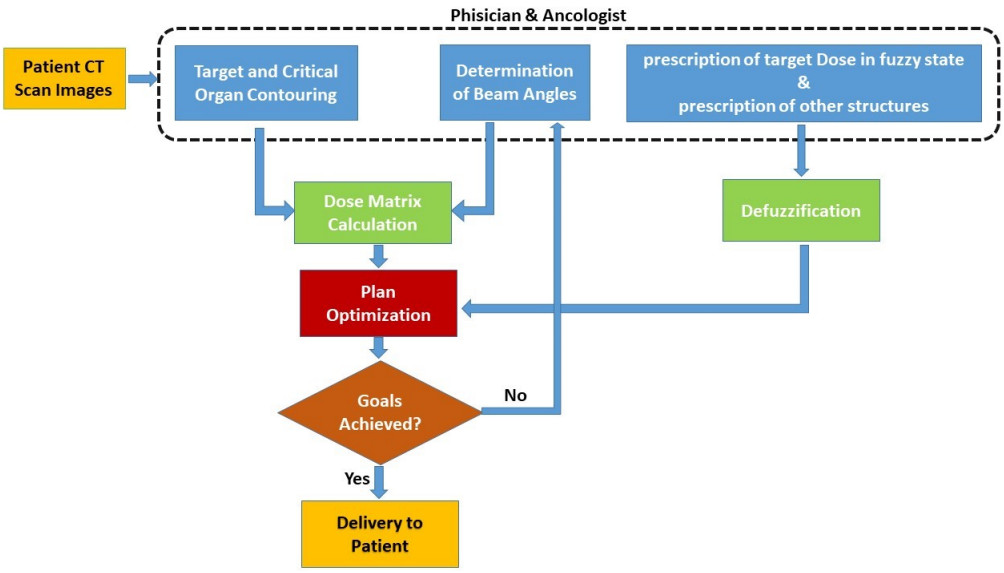

FIGURE 2. Flowchart for IMRT treatment planning on a fuzzy state.

prescription set H and the physical set K are defined as:

$$H = \left\{ \begin{bmatrix} \tilde{b}_t \\ u \end{bmatrix} : u \in D_v \right\} \subset \mathbb{R}_+^{m_t+m}, \qquad K = \left\{ \begin{bmatrix} A_t x \\ Ax + s \end{bmatrix} : x, s \geq 0 \right\} \subset \mathbb{R}_+^{m_t+m}.$$

Both H and K are closed sets in $\mathbb{R}_+^m$, and K is a convex cone; but H is non-convex since the DVCs have a combinatorial nature (Ripsman, Rahimi, et al. 2023). In fact, D_v is a non-convex union of convex boxes.

We would ideally like to find $x \in \mathbb{R}_+^n$ and $s \in \mathbb{R}_+^m$ that $A_t x = \tilde{b}_t$ and $Ax + s = u$. But the reality of the IMRT fluence problem is that there may be no physically achievable dose that both satisfies the DVCs and meets the prescription. That is, generally speaking $dist(H, K) > 0$, or equivalently, $H \cap K = \phi$; thus, the goal is to obtain $d_H \in H$and $d_K \in K$such that:

$$dist(H, K) = \|d_H - d_K\| = \min_{u \in D_v} \min_{x,s \geq 0} \left\| \begin{bmatrix} \tilde{b}_t \\ u \end{bmatrix} - \begin{bmatrix} A_t x \\ Ax + s \end{bmatrix} \right\|. \tag{3.1}$$

The norm in the right-hand side of 3.1 can be replaced by

$$q(x, s, u) = \frac{1}{2}\|A_t x - \tilde{b}_t\|^2 + \frac{1}{2}\|Ax + s - u\|^2; \tag{3.2}$$

thus, one can define our objective function as

$$f(u) = \min_{(x,s)\geq 0} q(x, s, u). \tag{3.3}$$

Now we represent the problem 3.1 with

$$\min_{u\in D_v} f(u). \tag{3.4}$$

It is not difficult to show that $f(u)$ decreases monotonically as u increases. Regardless the fact that the parameter $\tilde{b}_t$ is fuzzy, there are many methods for solving 3.4; to use the best one, we prefer first to de-fuzzify the problem.

4. De-fuzzify the problem

In order to solve 3.4 in a fuzzy environment, we need the following fuzzy concepts:

Definition 4.1. If the membership function of the fuzzy set $\tilde{A}$ on $\mathbb{R}$ be

$$\mu_{\tilde{A}}(x) = \begin{cases} (x-p)/(q-p), & p \leq x \leq q; \\ 1, & q \leq x \leq r; \\ (s-x)/(s-r), & r \leq x \leq s; \\ 0, & other, \end{cases}$$

where $p < q < r < s$, then $\tilde{A}$ is called a trapezoidal fuzzy number. We denote $\tilde{A} \equiv (p, q, r, s)$.

Definition 4.2. For each $a, b \in \mathbb{R}$, signed distance of a from$b$ is defined by $d^*(a, b) = a-b$. If a be in the right or the left of b, the sign of d^* will be negative or positive respectively. Also we have $d^*(a, b) = d^*(a, 0) - d^*(b, 0)$.

Definition 4.3. For $p < q$ and $0 < \alpha \leq 1$ if the membership function of the fuzzy set $[p_\alpha, q_\alpha]$ on $\mathbb{R}$ be

$$\mu_{[p_\alpha, q_\alpha]}(x) = \begin{cases} \alpha, & p \leq x \leq q; \\ 0, & otherwise, \end{cases} \tag{4.1}$$

then $[p_\alpha, q_\alpha]$ is called an α-level fuzzy interval. (See (Chiang 2001)).

As a fuzzy number, $\tilde{b}_i$ specifies the maximum and minimum dose absorbed for the voxel i of the target. For example, suppose that a prescription specifies the dose absorbed for the i voxel from 5Gy to 10Gy. These values have the most and least degree of satisfaction respectively, because, if the tumor absorbs less dose, then the organs at risk absorb less dose too. Let the degree of satisfaction be normalized as a membership degree, by $b_{i_{min}}$ with the membership degree 1 and $b_{i_{max}}$ with the membership degree zero and membership degree between 5Gy and 10Gy be1 (See Figure 3). To be able to consider as a trapezoidal fuzzy number, it is enough to select p in Definition 1 as a number that is very close to $b_{i_{min}}$, like $p = b_{i_{min}} - 10^{-5}$. Therefore, we consider $\tilde{b_i} = (b_{i_{min}} - 10^{-5}, b_{i_{min}}, \bar{b_i}, b_{i_{max}})$ that $\mu_{\tilde{b_i}}(y)$ is represented as below:

$$\begin{cases} \frac{(y-b_{i_{\min}}+10^{-5})}{10^{-5}}, & b_{i_{\min}} - 10^{-5} \leq y \leq b_{i_{\min}}; \\ 1, & b_{i_{\min}} \leq y \leq \bar{b_i}; \\ \frac{(b_{i_{\max}}-y)}{(b_{i_{\max}}-\bar{b_i})}, & \bar{b_i} \leq y \leq b_{i_{\max}}; \\ 0, & otherwise; \end{cases}$$

In the sense of [1], here, there exists an α-cut of $\tilde{b}_i$ for each $\alpha \in [0, 1]$; the left-hand point of an α-cut is $b_i^L(\alpha) = p + (q - p)\alpha$ and the right-hand point of it is $b_i^L(\alpha) = s - (s - r)\alpha$ (see Figure 3).

Therefore Corresponding to the crisp interval $[b_i^L(\alpha), b_i^U(\alpha)]$, we have the level α fuzzy interval $[b_i^L(\alpha)_\alpha, b_i^U(\alpha)_\alpha]$ (Chiang 2001). By 4.1 we have

$$\mu_{[b_i^L(\alpha)_\alpha, b_i^U(\alpha)_\alpha]}(x) = \begin{cases} \alpha, & b_i^L(\alpha) \leq x \leq b_i^U(\alpha); \\ 0, & otherwise, \end{cases}$$

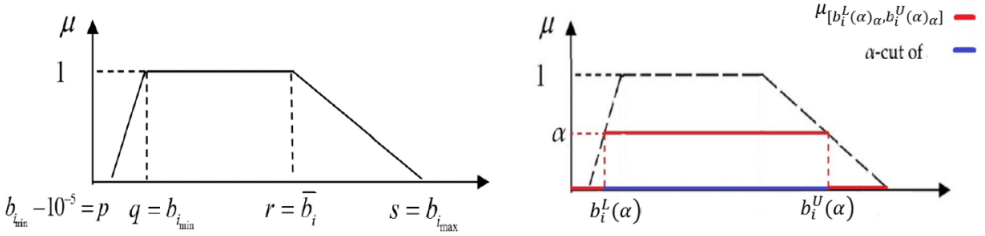

FIGURE 3. left) Membership function; right) α-cut of $\tilde{b_i}$

As previously mentioned, the influence matrix A_t and the vector x are crisp; thus, each component like $(A_t x)_i$ is also crisp. In the manner explained in (Chiang 2001), we define the signed distance of the crisp interval $[b_i^L(\alpha), b_i^U(\alpha)]$ to the crisp number $(A_t x)_i$ as:

$$\begin{aligned} d^*([b_i^L(\alpha), b_i^U(\alpha)], (A_t x)_i) &= \frac{1}{2}[d^*(b_i^L(\alpha), (A_t x)_i) + d^*(b_i^U(\alpha), (A_t x)_i)] \\ &= -(A_t x)_i + \frac{1}{2}[b_{i_{\min}} + b_{i_{\max}} + (\bar{b_i} - b_{i_{\max}})\alpha)]. \end{aligned}$$

Since the α- cut $[b_i^L(\alpha), b_i^U(\alpha)]$ and the α-level fuzzy interval $[b_i^L(\alpha)_\alpha, b_i^U(\alpha)_\alpha]$ are one to one correspondence, then one can define the signed distance of the α-level fuzzy interval $[b_i^L(\alpha)_\alpha, b_i^U(\alpha)_\alpha]$ from $(\tilde{A}_t x)_i$ by

$$d([b_i^L(\alpha)_\alpha, b_i^U(\alpha)_\alpha], (\tilde{A_t} x)_i) = d^*([b_i^L(\alpha), b_i^U(\alpha)], (A_t x)_i). \tag{4.2}$$

We remind that $(A_t x)_i$ is regarded as a fuzzy number by the usual one-to-one correspondence. The above function d is continuous respect to α in $[0, 1]$, now like (Chiang 2001) we can use a definite integral to find its average value. Therefore, we define the signed distance of $\tilde{b}_i$ from $(A_t x)_i$ as

$$d(\tilde{b_i}, (\tilde{A_t} x)_i) = \int_0^1 d^*([b_i^L(\alpha), b_i^U(\alpha)], (A_t x)_i) d\alpha = \frac{b_{i_{\min}}}{2} + \frac{\bar{b_i} + b_{i_{\max}}}{4} - (A_t x)_i. \tag{4.3}$$

We also introduce the following distance as a criterion for evaluating the proximity b_t and $A_t x$.

$$d(\tilde{b_t}, \tilde{A_t} x) = \sqrt{\sum_{i=1}^{m_t} (d(\tilde{b_i}, (\tilde{A_t} x)_i))^2}$$

Hence in fuzzy environment, 3.2 is converted to the following one:

$$q(x, s, u) = d(\tilde{b_t}, \tilde{A_t} x) + \frac{1}{2}\|Ax + s - u\|^2 = \frac{1}{2}\|A_t x - (\frac{b_{\min}}{2} + \frac{\bar{b} + b_{\max}}{4})\|^2 + \frac{1}{2}\|Ax + s - u\|^2,$$

thus by changing the fuzzy vector $\tilde{b_t}$ to a non-fuzzy vector b_t, the way of solving 3.4 in fuzziness state is the same as its crisp state, except that $\tilde{b_t}$ is replaced by $\frac{b_{min}}{2} + \frac{\bar{b} + b_{max}}{4}$.

5. Algorithm

For $u \in D_v$, one can prove that $f(u)$ is differentiable and that $\nabla f(u) = \nabla_u q(x(u), s(u), u) = -\max(Ax(u) - u, 0) \leq 0$, and that $s(u) = \max(u - Ax(u), 0)$. The derivation of this formula is rather long. The feasible set D_v is a non-convex set consisting of a large number of

"branches". Therefore, we can use the algorithm mentioned in (Merritt 2006) that seeks a "good" local minimum of 3.4 in an efficient manner. This algorithm uses a relaxation scheme based on the sensitivity of f and is called the Sensitivity-Driven Greedy (SDG) algorithm.

SDG Algorithm

Input: Initial dose $u^0 \in D_v$;

Output: Optimal beamlet intensities $x(u^k)$;

for $k = 0, 1, 2, \ldots$

Solve $f(u^k)$ for $x(u^k)$;

Compute $\nabla f(u^k) = -\max(Ax(u^k) - u^k, 0)$;

if stopping condition are met ($\|u^{k+1} - u^k\| < \varepsilon$),

the output is $x(u^k)$ and stop

else

Set $u^k + 1 = Proj_{D_v^k}(u^k - \nabla f(u^k))$, where $D_v^k = \{u : u \geq u^k\} \cap D_v$.

end if

end for

Our choice for u^0 is the prescribed dose bounds at the lowest level DVCs. Note that in Step 4 the vector inside the projection operator is

$$u^k - \nabla f(u^k) \equiv \max(u^k, Ax(u^k)) \geq u^k.$$

Hence, a dose bound u_i^k is replaced by the calculated dose value $[Ax(u^k)]_i$ whenever the latter is greater. The resulting larger vector is then projected onto the set D_v^k to obtain the next dose bound u^{k+1}. The following theorem shows that this algorithm is convergence (See (Merritt 2006)).

Theorem 5.1. *If A be full column rank, the Sensitivity-Driven Greedy Algorithm, without stopping, generates an infinite sequence $\{u_k\}$ that converges to a local minimum of f in D_v.*

The bulk of the computation in the SDG algorithm is to solve the sub-problem $Q(u^k)$ in Step 1 at each iteration which is a convex quadratic program known as a non-negative least-squares (NNLS) problem. Given their relatively large sizes in IMRT applications, a fast algorithm for solving these NNLS problems is of primary importance. On the

other hand, due to the errors in leaf-sequencing, measurement, imaging, dose calculation, patient motion, etc., high-accuracy solutions are not necessary. Like (Bahr, Kereiakes, et al. 1968), in our implementation, we use an interior-point gradient algorithm that was originally designed to strike a balance between reasonable accuracy and efficiency in this application.

6. Numerical Experiments

In our experiments, we used the QIB dose calculation engine native from CERR to generate an influence matrix for each test case using five equally-spaced beams. Our numerical experiments have been conducted on head-and-neck. (See Figure 4).

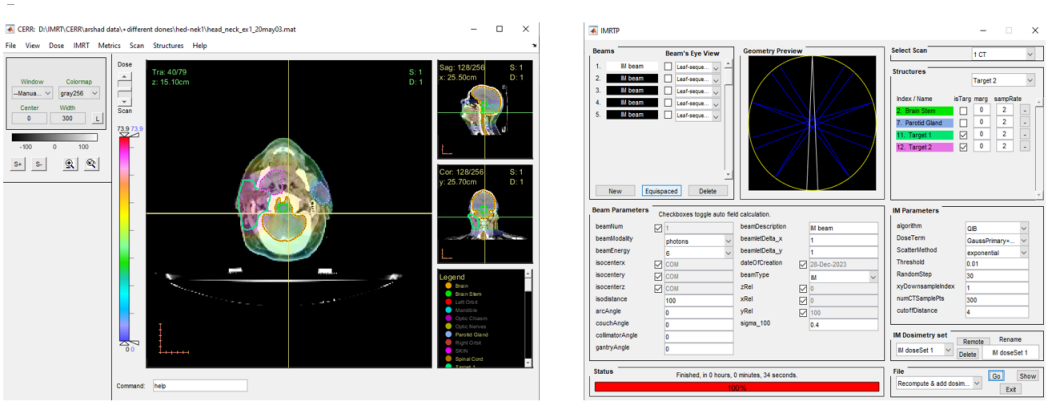

Figure 4. left) Importing scans for head and neck into CERR environment; right) IMRTP window in CERR environment for does calculation.

In IMRT, the DVC compliance is visualized by dose-volume histograms (DVHs), where the x-axis represents dose values and y-axis represents accumulated volume percentage. In the DVH, each planning structure has a corresponding curve. The ideal curve for a target structure is a step function dropping from 100 to zero at the prescribed dose value. For a healthy structure, the lower curve is better. On the other hand, a dose distribution satisfies the DVC if the curve is below or goes through the corresponding point. The DVC and DVH for the head-and-neck cancer case are given in Table 1 and Figure 5.

TABLE 1. The number of voxels and DVCs for head-and-neck case

Structures	The number of voxels	Prescribed dose	Volume
Target 1	5206	$\tilde{d}_t = (63 - 10^{-5}, 63, 75, 80)$	95%
Target 2	2412	$\tilde{d}_t = (56 - 10^{-5}, 56, 70, 75)$	95%
Brain Stem	671	23	45%
Parotid Glands	838	30	50%

TABLE 2. Dosimetric parameters of Target 1, Target 2, Brain Stem, and Parotid Glands for head-and-neck case in three methods

Structures	Evaluated Items	trapezoidal fuzzy target dose	CERR software
Target1	D_{min},	61.74	60.77
	D_{max}	68.64	74.07
	D_{mean}	66.47	69.20
	$D_{95\%}$	64.80	65.58
Target2	D_{min}	49.52	49.21
	D_{max}	66.29	71.12
	D_{mean}	60.48	60.71
	$D_{95\%}$	59.36	58.56
Brain Stem	D_{min}	0.88	0.79
	D_{max}	45.43	44.95
	D_{mean}	20.12	21.02
	$D_{95\%}$	21.05	18.83
Parotid Glands	D_{min}	8.12	3.8500
	D_{max}	37.47	54.8600
	D_{mean}	23.57	24.0600
	$D_{95\%}$	21.05	18.8300

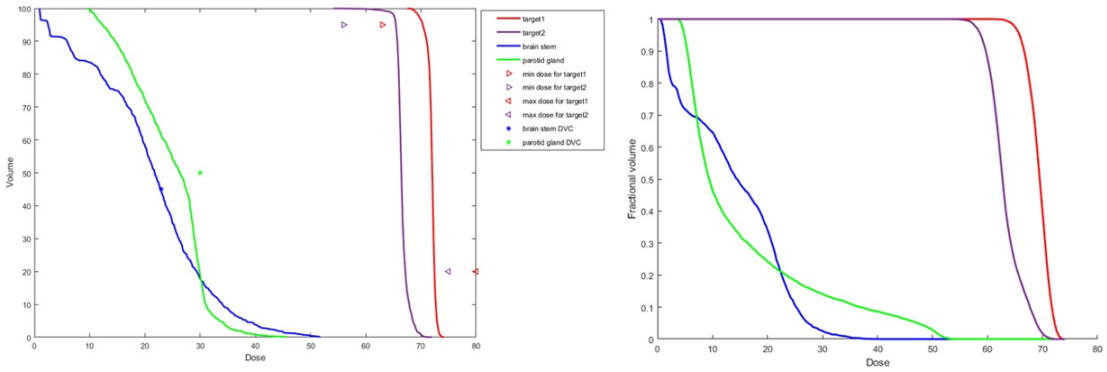

FIGURE 5. left) The obtained DVH of running Algorithm on the head-and-neck cancer case with prescribed trapezoidal fuzzy target dose; different colors are utilized to clarify the organs; right) The DVH is generated by the CERR software.

As shown in Figure 5, the curves of target 1 and target 2 in the trapezoidal fuzzy state have a better dose coverage related to the curves generated by the CERR software with the prescribed crisp target dose. According to the values of Dmax, Dmin, Dmean, D45%, and D50% in Table 2, in the CEER method, despite the relatively high dose coverage in the tumor structures, the Dmin in the parotid glands is significantly higher than the Dmin in trapezoidal method, which means that the CERR method causes more damage to this critical organ.

7. CONCLUSION

In the present article, a novel prescribed dose for target structure based on the concept of the trapezoidal fuzzy number in treatment planning was proposed. To verify its effectiveness, the proposed dose in the trapezoidal fuzzy number state was compared with the crisp state on a head-and-neck cancer case. Figure 5 left shows the optimization results for the head-and-neck cancer case with the prescribed trapezoidal fuzzy target dose in the DVH format, and Figure 5 right displays the DVH generated by the software CERR with the prescribed crisp target dose. In general, the obtained results show that the IMRT method with trapezoidal fuzzy target dose has better dose coverage in target structures and improves the quality of treatment planning.

References

[1] Bahr, G.K., Kereiakes, J.G., Horwitz, H., Finney, R., Galvin, J. and Goode, K., 1968. The method of linear programming applied to radiation treatment planning. *Radiology*, *91*(4), pp.686-693. doi: 10.1148/91.4.686.

[2] Breedveld, S., Storchi, P.R., Voet, P.W. and Heijmen, B.J., 2012. iCycle: Integrated, multicriterial beam angle, and profile optimization for generation of coplanar and noncoplanar IMRT plans. *Medical physics*, *39*(2), pp.951-963. doi: 10.1118/1.3676689.

[3] Chiang, J., 2001. Fuzzy linear programming based on statistical confidence interval and interval-valued fuzzy set. *European Journal of Operational Research*, *129*(1), pp.65-86. doi: 10.1016/S0377-2217(99)00404-X

[4] Cotrutz, C., Lahanas, M., Kappas, C. and Baltas, D., 2001. A multiobjective gradient-based dose optimization algorithm for external beam conformal radiotherapy. *Physics in Medicine & Biology*, *46*(8), p.2161. doi: 10.1088/0031-9155/46/8/309

[5] Deasy, J., 2010. Computational environment for radiotherapy research. *St. Louis*, MO. doi: 10.1118/1.1568978

[6] Devarajan, D., Alex, D.S., Mahesh, T.R., Kumar, V.V., Aluvalu, R., Maheswari, V.U. and Shitharth, S., 2022. Cervical cancer diagnosis using intelligent living behavior of artificial jellyfish optimized with artificial neural network. *IEEE Access*, *10*, pp.126957-126968. doi: 10.1109/ACCESS.2022.3221451

[7] Fakharzadeh Jahromi, A., Bozorg, O., Maleki, H. and Mosleh-Shirazi, M.A., 2011. Fluence map optimization in intensity modulated radiation therapy for fuzzy target dose. *Iranian Journal of Fuzzy Systems*, *8*(4), pp.93-105. doi: 10.22111/IJFS.2011.310

[8] Fallahi, A., Mahnam, M. and Niaki, S.T.A., 2022. A discrete differential evolution with local search particle swarm optimization to direct angle and aperture optimization in IMRT treatment planning problem. *Applied Soft Computing*, *131*, p.109798. doi: 10.1016/j.asoc.2022.109798

[9] de Freitas, J.C., de Oliveira Florentino, H., dos Santos Benedito, A. and Cantane, D.R., 2020. Optimization model applied to radiotherapy planning problem with dose intensity and beam choice. *Applied Mathematics and Computation*, *387*, p.124786. doi: 10.1016/j.amc.2019.124786

[10] Fu, Y., Zhang, H., Morris, E.D., Glide-Hurst, C.K., Pai, S., Traverso, A., Wee, L., Hadzic, I., Lønne, P.I., Shen, C. and Liu, T., 2021. Artificial intelligence in radiation therapy. *IEEE transactions on radiation and plasma medical sciences*, *6*(2), pp.158-181. doi: 10.1109/TRPMS.2021.3107454

[11] Merritt, M.S., 2006. A sensitivity-driven greedy approach to fluence map optimization in intensity-modulated radiation therapy. *Rice University*.

[12] Ripsman, D.A., Rahimi, F., Abouee-Mehrizi, H. and Mahmoudzadeh, H., 2023. Light Pareto robust optimization for IMRT treatment planning. *Medical Physics*, *50*(5), pp.2637-2648. doi: 10.1002/mp.16298

[13] Sadegheih, A., Savari, M. and Nickfarjam, A., 2018. Using Mixed Integer Linear Programming Model For Beam Angle And Fluence Map Optimization In Intensity Modulated Radiation Therapy. *SSU_Journals*, *26*(1), pp.27-39.

[14] Selvarajan, S., Manoharan, H., Hasanin, T., Alsini, R., Uddin, M., Shorfuzzaman, M. and Alsufyani, A., 2022. Biomedical signals for healthcare using Hadoop infrastructure with artificial intelligence and fuzzy logic interpretation. *Applied Sciences*, *12*(10), p.5097. doi: 10.3390/app12105097

[15] Shepard, D.M., Ferris, M.C., Olivera, G.H. and Mackie, T.R., 1999. Optimizing the delivery of radiation therapy to cancer patients. *Siam Review*, *41*(4), pp.721-744. doi: 10.1137/S0036144598342032

[16] Shitharth, S., Yonbawi, S., Manoharan, H., Alahmari, S., Yafoz, A. and Mujlid, H., 2023. Physical stint virtual representation of biomedical signals with wireless sensors using swarm intelligence optimization algorithm. *IEEE Sensors Journal*, *23*(4), pp.3870-3877. doi: 10.1109/JSEN.2022.3233407

[17] Teichert, K., Currie, G., Küfer, K.H., Miguel-Chumacero, E., Süss, P., Walczak, M. and Currie, S., 2019. Targeted multi-criteria optimisation in IMRT planning supplemented by knowledge based model creation. *Operations Research for Health Care*, *23*, p.100185. doi: https://doi.org/10.1016/j.orhc.2019.04.003

[18] Webb, S., 1989. Optimisation of conformal radiotherapy dose distribution by simulated annealing. *Physics in Medicine & Biology*, *34*(10), p.1349. doi: 10.1088/0031-9155/34/10/002

Omolbanin Bozorg
Department of Mathematics,
Yazd University,
Yazd, Iran
Email: o.bozorg@gmail.com,

Alireza Fakharzadeh Jahromi
Department of Mathematics,
Shiraz University of Technology,
Shiraz, Iran
Email: a_fakharzadeh@sutech.ac.ir

Ali Delavar Khalafi
Department of Mathematics,
Yazd University,
Yazd, Iran
Email: delavarkh@yazd.ac.ir